Nanoscale

Cite this: *Nanoscale*, 2012, **4**, 2150

www.rsc.org/nanoscale

PAPER

Synthesis of hydrothermally stable, hierarchically mesoporous aluminosilicate Al-SBA-1 and their catalytic properties

Na Li, Jin-Gui Wang, Jian-Xiong Xu, Jin-Yu Liu, Hui-Jing Zhou, Ping-Chuan Sun and Tie-Hong Chen*

Received 2nd November 2011, Accepted 16th January 2012
DOI: 10.1039/c2nr11643j

Hydrothermally stable mesoporous aluminosilicates Al-SBA-1 with hierarchical pore structure have been successfully synthesized under alkaline condition at 120 °C by employing organic mesomorphous complexes of polyelectrolyte (poly(acrylic acid) (PAA)) and cationic surfactant (hexadecyl pyridinium chloride (CPC)) as template. The Si/Al ratio could be as high as 5 and the incorporation of Al into the silica framework did not disturb the well-ordered cubic $Pm\bar{3}n$ mesostructure. Meanwhile, the incorporation of Al could greatly increase the specific surface area and pore volume of the samples. The Al-SBA-1 materials exhibited a high hydrothermal stability and remained stable even after being treated in boiling water for 10 days. The catalytic activity of the Al-SBA-1 materials was investigated by employing the Friedel–Crafts alkylation of toluene with benzyl alcohol as a model reaction and they exhibited excellent catalytic property due to the incorporated acid sites and the hierarchically mesoporous structure.

1. Introduction

Mesoporous materials with three dimensional (3-D) porous structures have been of growing interest in recent years due to their potential applications.[1–3] Compared to the materials with hexagonal pore structure with one dimensional pore system, the advantage of the 3-D pore system materials is the resistance to pore blocking and easy diffusion of reactants inside the porous channels. Up to now, several mesoporous materials with 3-D pore systems have been reported, such as SBA-1, FDU-1, AMS-8 and SBA-16.[4–9] Among them, mesoporous silica SBA-1 is an interesting material which possesses a cage-type structure with 3-D interconnected small open windows.[10–12]

Recently, hierarchically porous materials with well-defined morphologies have attracted much attention in the fields of catalysis, separation, adsorption and biomedicine owing to their excellent textural characteristics such as a hierarchically porous structure, high surface area and large pore volume.[13–18] Nevertheless, a main drawback of these materials with pure silica framework is that they often display relatively poor hydrothermal stability, which will restrain their extensive industrial application. During the past few decades, great efforts have been made to improve the hydrothermal stability of the mesoporous materials,[19–32] such as the addition of salt in synthesis,[19–21] increasing the pore wall thickness,[22] incorporation of heteroatom by *in situ* or post-grafting,[23–27] pH adjusting,[23,28] assembly of preformed zeolite seeds[29–31] and so on. However, the synthesis of hierarchically porous materials with enhanced hydrothermal stability is still a great challenge.

It is well-known that the incorporation of heteroatoms especially for Al species in the silica framework has been proved to be an efficient method to enhance the hydrothermal stability and create more catalytic active sites in the materials.[23–27] Usually, the synthesis of Al-SBA-1 is achieved under acidic condition.[33–36] However, the acidic condition does not favor the incorporation of metallic species in the silica framework, which often leads to low metal loading amounts, low hydrothermal stability or extra-framework species instead of isomorphous substitution for the silicon sites. Recently, Cheng *et al.* demonstrated a successful synthesis of Al-SBA-1 under alkaline conditions (pH around 9) at a temperature of 0 °C.[37]

In our previous study,[38] we reported the synthesis of hollow carved single-crystal mesoporous silica SBA-1 under alkaline condition. In this manuscript, hydrothermally stable single-crystal mesoporous aluminosilicates Al-SBA-1 with hierarchical pore structure have been successfully synthesized under alkaline condition (at pH = 10–11) by employing organic mesomorphous complexes of polyelectrolyte (poly(acrylic acid) (PAA)) and cationic surfactant (hexadecyl pyridinium chloride (CPC)) as template, and aluminium isopropoxide as Al source at a high aging temperature of 120 °C. A high level of Al incorporation with an Si/Al ratio of up to 5 was achieved. The Al-SBA-1 materials retained the well-ordered cubic $Pm\bar{3}n$ mesostructure and presented higher specific surface area and pore volume. Hydrothermal treatment shows that the Al-SBA-1 materials exhibited a high hydrothermal stability even after being treated in boiling water for 10 days. Catalyzed Friedel–Crafts alkylation of toluene with benzyl alcohol demonstrated

Institute of New Catalytic Materials Science, Key Laboratory of Advanced Energy Materials Chemistry (MOE), College of Chemistry, Nankai University, Tianjin 300071, PR China. E-mail: chenth@nankai.edu.cn

that the Al-SBA-1 materials showed excellent catalytic properties due to the incorporated acid sites and the hierarchically nanoporous structure.

2. Experimental

2.1 Chemicals and materials

Hexadecyl pyridinium chloride (CPC) and aluminium isopropoxide were obtained from Aladdin, China. Poly(acrylic acid) (PAA) (average molecular weight 240 000, 25% solution in water) was from Acros. In this work the amount of PAA used in the synthesis means the weight of the PAA solution. Tetraethylsiloxane (TEOS) was purchased from Alfa Aesar. All the chemical agents were used without further purification.

2.2 Synthesis of hierarchically mesoporous SBA-1

The pristine siliceous SBA-1 was firstly synthesized based on the reported method.[38] Typically, 0.54 g of CPC was dissolved in 25 mL of deionized water under stirring, and then 3.0 g of PAA solution was added under vigorous stirring at room temperature to obtain a clear solution. Next, 4.0 g of ammonia solution (25%) was added to the above solution under vigorous stirring. After further stirring for 20 min, 2.08 g of tetraethylsiloxane (TEOS) was added to the above suspension. The mixture was stirred for another 15 min, and then was transferred into an autoclave which was placed in an oven at 120 °C for 96 h. The final product was centrifuged, washed with deionized water, and dried at 60 °C. The organic templates were removed by calcination at 550 °C for 5 h.

2.3 Synthesis of hierarchically mesoporous Al-SBA-1

The Al-SBA-1 samples with different Si/Al molar ratios were synthesized *via* a one step method under the same procedure by using aluminium isopropoxide as Al source. For a typical preparation, 0.54 g of CPC, 25 mL of H_2O, 3.0 g of PAA and 4.0 g of ammonia solution were added into a glass flask with vigorous stirring, then 2.08 g of tetraethylsiloxane (TEOS) and a certain amount of aluminium isopropoxide (with the TEOS/aluminium isopropoxide molar ratio of 50, 20 and 10) were added. The mixture was stirred for 3 h, and finally transferred into an autoclave which was left in a 120 °C oven for 4 days. The final product was centrifuged, dried, and calcined. The samples were denoted as Al-SBA-1-*x* and (where *x* indicates the molar ratio of Si/Al in the initial solution).

2.4 Hydrothermal stability evaluation

The hydrothermal stability of the samples was investigated by treating calcined SBA-1 and Al-SBA-1 in boiling water. Typically, 0.3 g of the calcined sample was added in 30 mL deionized water in a closed autoclave at 100 °C for 10 days under static conditions. The samples were filtered, without washing, and dried at 50 °C overnight. The steamed sample was denoted as Al-SBA-1-*x*-HT.

2.5 Catalytic properties of the hierarchically mesoporous Al-SBA-1

Here we choose Friedel–Crafts alkylation of toluene with benzyl alcohol as the model reaction to test the catalytic properties of the hierarchical Al-SBA-1. The liquid phase benzylation of toluene with benzyl alcohol was carried out in a three-necked flask equipped with a reflux condenser, heated in a temperature-controlled oil bath (110 °C) under atmospheric pressure. In a typical run, 4.5 g of toluene and 0.25 g of benzyl alcohol were firstly added into a three-necked flask equipped with a reflux condenser and followed by adding 0.035 g of catalyst. The catalytic reaction was performed in a temperature-controlled oil bath (110 °C) under atmospheric pressure. Samples were withdrawn at regular intervals and then centrifuged. The liquid supernatant was analyzed by gas chromatograph (GC-7800) with a flame ionization detector, using a FFAP and N_2 as carrier gas. The conversion was calculated based on benzyl alcohol.

2.6 Characterization

Small-angle X-ray scattering (SAXS) experiments were performed on a Bruker Nanostar small angle X-ray scattering system. Scanning electron microscopy (SEM) images were obtained with a Shimadzu SS-550 instrument. Transmission electron microscopy (TEM) observations were performed on a Philips Tecnai F20 microscope, working at 200 kV. All samples subjected to TEM measurements were dispersed in ethanol ultrasonically and were dropped on copper grids. N_2 adsorption measurements were performed on a BELSORP-mini II sorption analyzer. The specific surface area was calculated by the BET (Brunauer–Emmett–Teller) method, the pore size distribution was calculated from the adsorption branch using the BJH (Barett–Joyner–Halenda) method and the total pore volume was obtained at a relative pressure of $p/p_0 = 0.99$. Before measurements, the samples were dried under dry N_2 flow at 350 °C for 5 h. Elemental analysis for Si/Al ratios was performed with inductively coupled plasma atomic emission spectroscopy (ICP-AES) using a Thermo Jarrell-Ash ICP-9000(N + M). ^{27}Al MAS NMR spectra were measured with a spin rate of 12 kHz, a contact time of 0.8 ms, and a recycle delay of 3 s. Ammonia temperature programmed desorption (NH_3-TPD) measurements were carried out on Micromeritics Chemisorption Analyzer (USA). Before measurements, the samples were firstly activated at 600 °C for 1 h under helium atmosphere. After the temperature cooled down to 50 °C, the sample was swept with ammonia for 1 h, then the gas was switched to helium to remove the physically adsorbed ammonia molecules, until the baseline was flat. After this, the temperature was increased to 600 °C with a ramping rate of 10 °C min^{-1} to obtain the NH_3-TPD curves.

3. Results and discussion

In our synthesis, a series of Al-SBA-1 samples with different Si/Al molar ratios were synthesized under alkaline condition by employing organic mesomorphous complexes of PAA and cationic surfactant CPC as templates, and aluminium isopropoxide as Al source at a high aging temperature (120 °C). Fig. 1 shows the small-angle X-ray scattering (SAXS) patterns of the calcined SBA-1 and Al-SBA-1 samples. As shown, three well

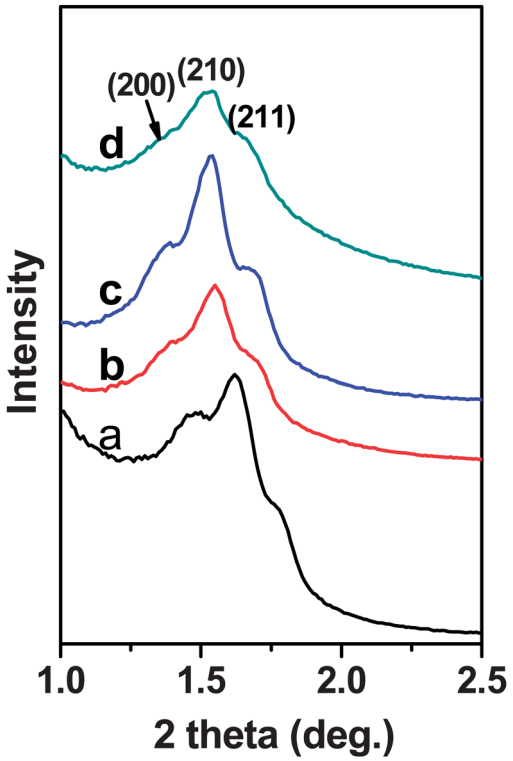

Fig. 1 SAXS patterns of the calcined samples: (a) SBA-1, (b) Al-SBA-1-50, (c) Al-SBA-1-20, (d) Al-SBA-1-10.

resolved diffraction peaks, which were indexed to the (200), (210) and (211) character diffractions of the cubic $Pm\bar{3}n$ mesostructure of SBA-1, are clearly observed (Fig. 1a). The shape of the SAXS patterns of the Al-SBA-1 (Fig. 1b–d) is similar to that of the SBA-1, indicating that the three dimensional cubic cage-type structure of the SBA-1 is retained well after incorporation of aluminium in silica materials. Moreover, it is observed that the increase of the Al content in the samples caused a shift of all reflections to lower angle, which reveals an increase in the d-spacing of the samples (Table 1). The unit cell parameter of the Al-SBA-1-10 material (12.8 nm) calculated by using the formula $a_0 = d_{210}\sqrt{5}$ is larger than that of the SBA-1 (12.2 nm).

The morphologies of the SBA-1 and Al incorporated SBA-1 samples were characterized by SEM. Here, we choose the Al-SBA-1-10 as a typical example. Fig. 2 shows the SEM images of the SBA-1 (Fig. 2a) and Al-SBA-1-10 (Fig. 2b). As was shown in Fig. 2a, the SBA-1 exhibited submicrometer spherical morphology with a particle size range of 200–500 nm. Similar features were observed with the samples of Al-SBA-1-10 (Fig. 2b).

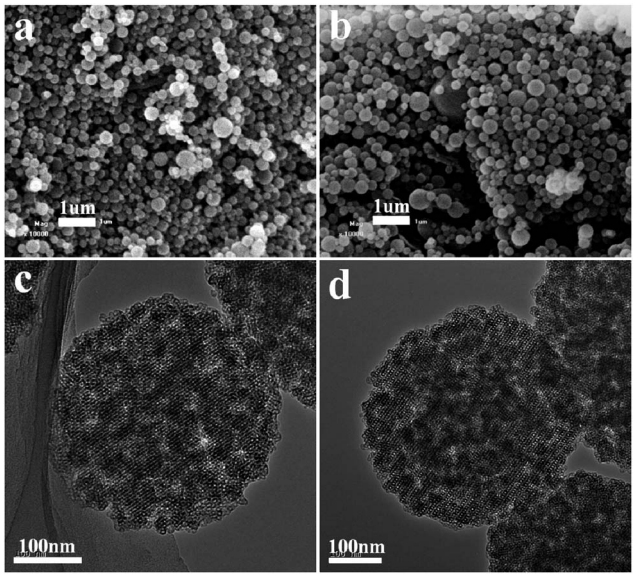

Fig. 2 SEM and TEM images of the calcined samples: (a, c) SBA-1, (b, d) Al-SBA-1-10.

This indicates that the incorporation of aluminium in SBA-1 has no evident effect on the morphology of the samples. In order to further examine the interior texture and pore structure of the samples, the SBA-1 and Al-SBA-1-10 were characterized by TEM, as shown in Fig. 2c and Fig. 2d, respectively. The Al-SBA-1-10 displayed the presence of interstitial nanopores inside the submicrospheres as well as ordered alignment of mesopores through the whole particle, indicating that the incorporation of Al into the silica framework did not significantly disturb the interior texture and pore structure of the SBA-1.

The nitrogen adsorption–desorption isotherms and pore size distribution curves of the SBA-1 and Al-SBA-1 samples are shown in Fig. 3. All the samples exhibited type IV isotherms with adsorption steps at relative pressures of 0.3–0.5, 0.75–0.95 and 0.95–0.99, respectively. The first step at a relative pressure of 0.3–0.5 (indicated by the dotted line in Fig. 3A) gives rise to the relatively narrow peaks at about 3 nm in the pore size distribution curves (Fig. 3B), corresponding to the cage-like mesopores of SBA-1. The second adsorption step between 0.75–0.95 gives rise to a broad pore size distribution centered at 43, 48, 39, and 48 nm, respectively, corresponding to the interstitial nanopores as observed in TEM images. The third adsorption step corresponded to a broad pore size distribution centered at about 100 nm, which was ascribed to the aggregated voids between the

Table 1 Structural parameters of the calcined SBA-1 and Al-SBA-1 samples

Sample	Si/Al in product[b]	d_{210}/nm	a_0[c]/nm	BET surface area/m^2 g^{-1}	Mesopore size/nm	Nanopore size/nm	Pore volume/cm^3 g^{-1}
SBA-1	—	5.44	12.2	134	2.6	43	1.03
Al-SBA-1-50[a]	23	5.69	12.7	238	3.2	48	1.32
Al-SBA-1-20[a]	14	5.74	12.8	390	3.2	39	1.35
Al-SBA-1-10[a]	5	5.74	12.8	477	3.4	48	1.47

[a] The number indicates the molar ratio of TEOS and aluminium isopropoxide in the synthesis. [b] The actual Si/Al mole ratios in the calcined products measured by ICP-AES. [c] Unit cell parameter.

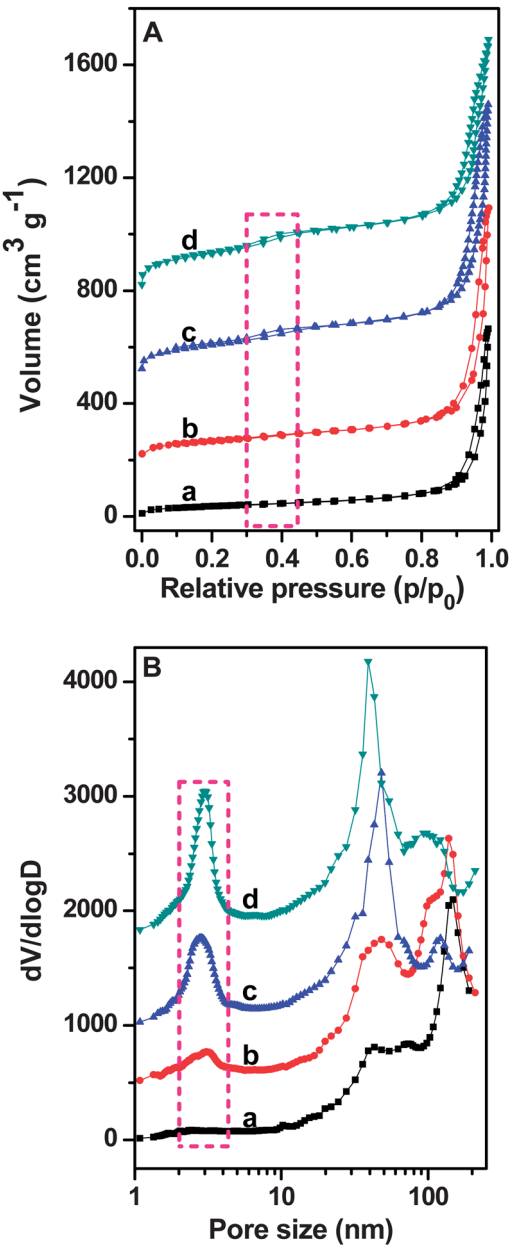

Fig. 3 (A) Nitrogen adsorption–desorption isotherms and (B) pore size distribution curves of the calcined samples: (a) SBA-1, (b) Al-SBA-1-50, (c) Al-SBA-1-20, (d) Al-SBA-1-10.

particles. As shown in Fig. 3A, with the increase of the Al content the first step of 0.3–0.5 became gradually pronounced. This phenomenon is in accordance with the increase of about 3 nm mespores shown in pore size distribution curves. The textural parameters such as specific surface area, pore volume and pore size are given in Table 1. The Al-SBA-1 samples exhibit surface area in the range of 238–477 $m^2 g^{-1}$, pore volume in the range of 1.32–1.47 $cm^3 g^{-1}$ and mesopore size ranging from 3.2 to 3.4 nm. On the other hand, the specific surface area, pore volume, and mesopore size of SBA-1 are 134 $m^2 g^{-1}$, 1.03 $cm^3 g^{-1}$, and 2.6 nm, respectively. During the synthesis, with the increase of the Al source, the interaction between the Al species and the CPC micelles would influence the co-assembly of the inorganic species with the template as well as the cross-linking of the silica framework, thus giving rise to larger *d* spacing, mesopore size and specific area.

Generally, the incorporation of Al into the framework of the mesoporous silica materials will create acidic sites in the mesoporous materials. It is believed that the amount of aluminium in the framework as well as its coordination determines the acidity of the sample.[39] In order to investigate the acidic properties of the obtained materials, several methods have been used. The amounts of the elements Al and Si of Al-SBA-1 were measured by ICP-AES and the results are presented in Table 1. The Si/Al molar ratio of the calcined samples increase with the increasing Si/Al in the synthesis solution (Table 1). ^{27}Al MAS NMR spectra allowed identification of the coordination state of aluminium in the silicate framework. Fig. 4 shows the ^{27}Al MAS NMR spectra of the calcined Al-SBA-1 samples. The signals at 54, 30 and 0 ppm corresponded to the tetrahedrally (Al(IV)), penta- (Al(V)) and octahedrally (Al(VI)) coordinated Al species, respectively. The tetrahedrally coordinated and the octahedrally coordinated aluminium species were associated with Brønsted acid sites and Lewis acid sites. As shown in Fig. 4, the incorporated Al atoms in the silica framework mainly exist in the form of Al(IV) and with the increase of the Al content, the Al(IV) was gradually transformed to Al(V) and Al(VI) species. The acid strength of the samples was investigated by NH_3-TPD, as shown in Fig. 5. The low temperature peak at around 100 °C was due to weak acid sites while the high temperature peak, appearing at about 300 °C corresponded to medium acid sites. It can be seen in Fig. 5, both the weak and medium acid sites increased with the Al content. Moreover, the low temperature peak shifts to higher temperature with the increase of the Al content, indicating the increase of the acid strength. Fig. 5d represents the NH_3-TPD curve of the commercial HZSM-5 (Si/Al = 25). Three peaks at 125, 200, 400 °C are observed, indicating the amount of ammonia desorbed from HZSM-5 is higher than that of the Al-SBA-1.

Hydrothermal stability is considered an important parameter for materials that would be applied as catalysts in reactions where water is produced or need to be regenerated in the presence of water vapor. In our system, the Al-SBA-1 was synthesized at

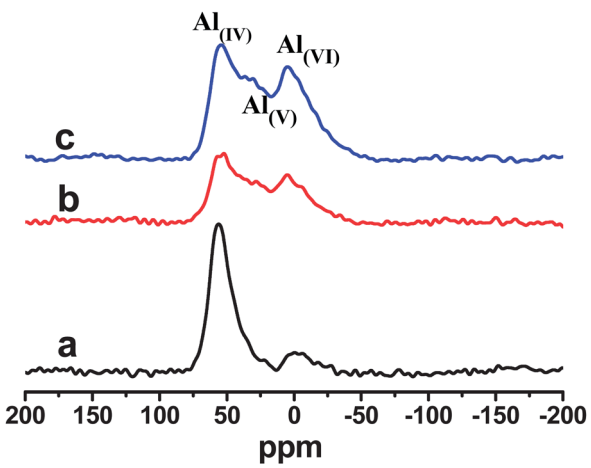

Fig. 4 ^{27}Al MAS NMR spectra of the calcined samples: (a) Al-SBA-1-50, (b) Al-SBA-1-20, (c) Al-SBA-1-10.

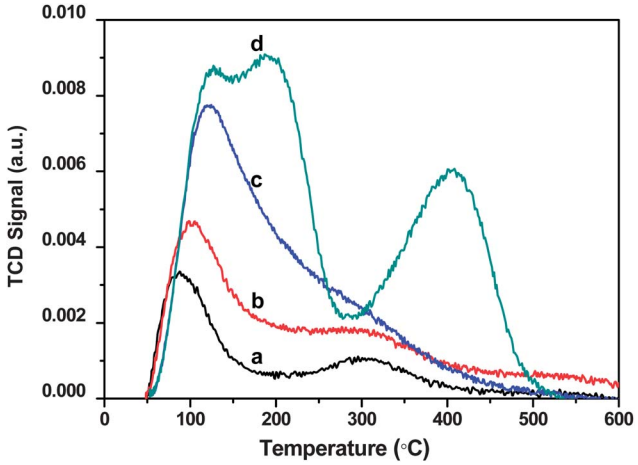

Fig. 5 NH_3-TPD curves of the calcined samples: (a) Al-SBA-1-50, (b) Al-SBA-1-20, (c) Al-SBA-1-10, (d) commercial HZSM-5.

a temperature of 120 °C and these as-prepared materials are expected to have a better hydrothermal stability. In order to check the hydrothermal stability of the SBA-1 and Al-SBA-1, the calcined samples were subjected to hydrothermal treatment in an autoclave at 100 °C for 10 days. Fig. 6 shows the SAXS patterns of SBA-1-HT and Al-SBA-1-HT samples. As shown in Fig. 6a, no diffraction peak for the SBA-1-HT was detected after hydrothermal treatment, indicating that its mesostructure has been severely destructed. This was mainly due to the fact that during the hydrothermal treatment process, the ≡Si–O–Si≡ in the framework can be hydrolyzed into ≡Si–OH. However, the Al-SBA-1-HT still exhibited three well-resolved diffraction peaks

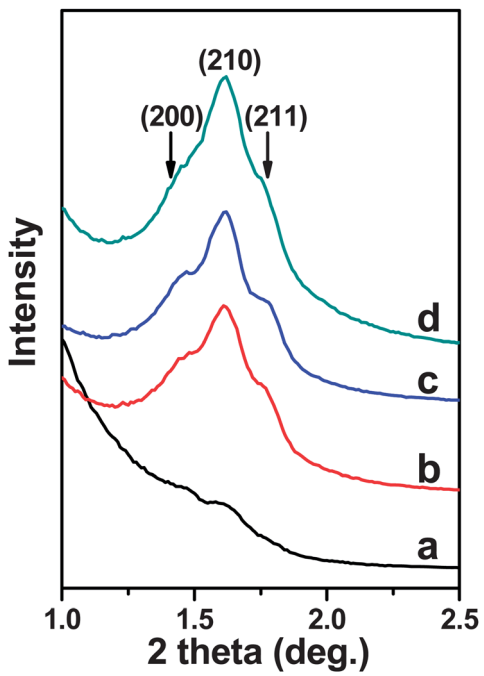

Fig. 6 SAXS patterns of the calcined Al-SBA-1 samples after 100 °C hydrothermal treatment for 10 days. (a) SBA-1-HT, (b) Al-SBA-1-50-HT, (c) Al-SBA-1-20-HT, (d) Al-SBA-1-10-HT.

(Fig. 6b–d) after the same treatment indicating the $Pm\bar{3}n$ mesostructure was well retained. Fig. 7 and Fig. 8 show the TEM images and N_2 adsorption–desorption isotherms of Al-SBA-1-10-HT samples. The TEM images show that the hierarchically mesoporous structure was retained after hydrothermal treatment. Furthermore, the N_2 adsorption isotherm still exhibits typical type IV isotherms and in the pore size distribution curve (Fig. 8) there appeared three peaks corresponding to the ordered mesopore, secondary interstitial nanopores and aggregated voids between the particles. The BET surface area and pore volume of the Al-SBA-1-10-HT were 308 $m^2\ g^{-1}$ and 1.09 $cm^3\ g^{-1}$, respectively, which is lower than that of the Al-SBA-1-10. This was mainly due to the fact that a small portion of the pore collapsed during the hydrothermal treatment. The results suggest that the synthesized Al-SBA-1 materials have a remarkable hydrothermal stability. The ≡Si–O–Al≡ bonds formed on the pore surface are more stable than the ≡Si–O–Si≡ bonds, and this would contribute to the hydrothermal stability of the Al-SBA-1 materials. Previous studies demonstrated that the surface layer of aluminosilicate could function as a protective layer in two ways: on the one hand, it protects the aluminosilicate framework from the attack of water molecules by blocking the terminal –OH group and ≡Si–O–Si≡ bonds on the surface of material. On the other hand, the negative charge of the aluminosilicate layer repels the access of OH^- ions, which catalyzes the hydrolysis procedure of the silica framework.[31,42,43]

Friedel–Crafts alkylation is an industrially important reaction used to produce numerous aromatic compounds. Various aluminosilicate catalysts such as zeolite beta, zeolite Y, MCM-41 and other mesoporous materials have been shown to be active for alkylation of benzene or toluene.[40,41] It is deemed that the activity of the catalysts is dependent on the mass transport and active sites.[39] Materials with hierarchical pore structure with two or three length scale pores was considered as an ideal catalyst.[26] Herein, the hierarchically mesoporous aluminosilicates Al-SBA-1 are utilized to catalyse the benzylation of toluene with benzyl alcohol. The main product and by-product of the benzylation is benzyl toluene (BT) and benzyl ester (BE), which are shown in Scheme 1. Commercial HZSM-5 with micropore but high acidity was chosen as the reference catalyst to investigate the effect of mass transfer on catalytic activity. Table 2 summarizes the catalytic activity and selectivity of the different Al-SBA-1 samples and HZSM-5. For all the Al-SBA-1 catalysts, the conversion reached 100% after 180 min, while the conversion for HZSM-5 was only 9% after 180 min. This was mainly due to the

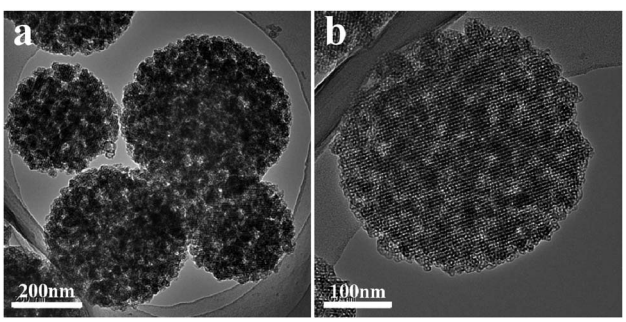

Fig. 7 TEM images of the Al-SBA-1-10-HT.

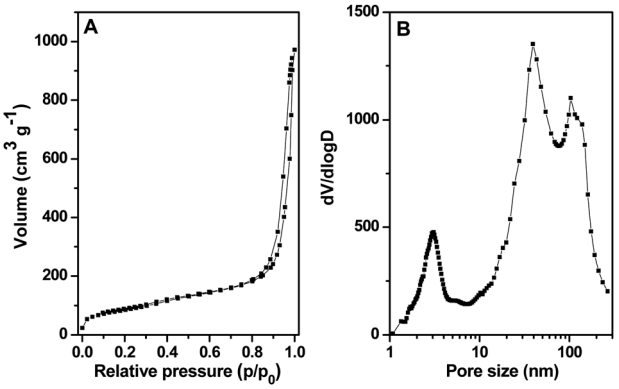

Fig. 8 (A) Nitrogen adsorption–desorption isotherms and (B) pore size distribution of the Al-SBA-1-10-HT sample.

Table 2 Performance of the Al-SBA-1 and commercial HZSM-5 in the benzylation of toluene with benzyl alcohol

Catalysts	Time/min	C_{BzOH}[a] (%)	S_{BT}[b] (%)	S_{BE}[c] (%)
Al-SBA-1-50	60	70	62	38
	120	90	68	32
	180	100	72	22
Al-SBA-1-20	60	77	61	39
	120	100	74	26
	180	100	79	21
Al-SBA-1-10	60	99	70	30
	120	100	83	17
	180	100	91	9
Al-SBA-1-10-HT	60	98	49	51
	120	100	76	24
	180	100	89	11
HZSM-5	180	9	6	94

[a] The conversion of benzyl alcohol [b] The selectivity to benzyl toluene [c] The selectivity to benzyl ester

smaller pore size (<1 nm) of the HZSM-5 which caused mass transfer limitation. In order to verify the effect of acid site concentration in the Al-SBA-1 catalysts, we investigate the catalytic activity of the Al-SBA-1 catalysts of different Al content. As indicated in Table 2, both the catalytic reaction rates and the selectivity to BT rise with the increase of the Al content in the Al-SBA-1 catalysts. For the Al-SBA-1-10 catalyst, the conversion of benzyl alcohol reached 99% in 60 min and the selectivity reached as high as 91% after 180 min. However, for Al-SBA-1-20 and Al-SBA-1-50 catalysts, the conversion of benzyl alcohol reached 100% in 120 min and 180 min and the selectivity was only 72% and 79% after 180 min, respectively. This suggests that more acidic sites efficiently promotes the catalytic activity.

The recycling of Al-SBA-1 catalysts have also been studied. Here we choose the Al-SBA-1-10 as a typical example. After the benzylation of toluene with benzyl alcohol is just completed in 60 min, the catalyst was filtered, washed several times with toluene and ethanol and then vacuum dried. The separated catalyst was reused in the next run. It is found that the conversion of benzyl alcohol was about 97% after three cycles and 91% after four cycles of benzylation (Fig. 9). The recycled catalyst was further characterized by TEM and ICP-AES. As shown in Fig. 10, the morphology and the pore structure of the Al-SAB-1-10 after recycling remained similar to the fresh catalyst, suggesting the

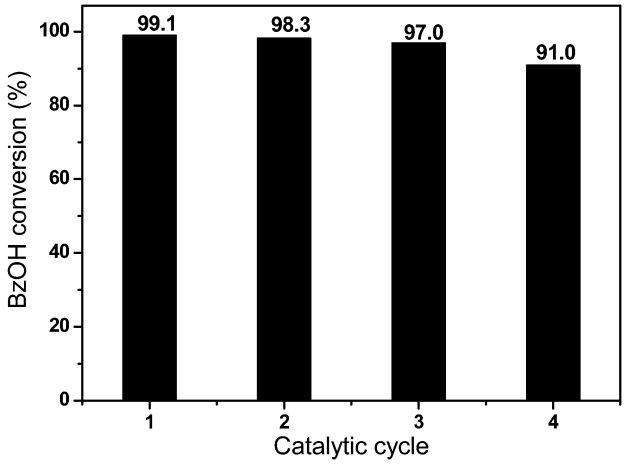

Fig. 9 Recyclability studies of Al-SBA-1-10 in the benzylation of toluene with benzyl alcohol.

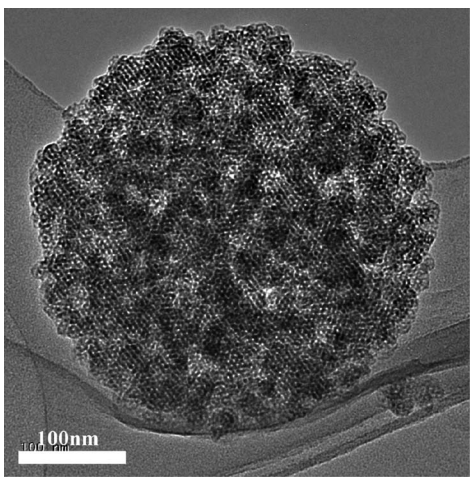

Fig. 10 TEM image of the recycled Al-SBA-1-10 catalyst.

reusability of the Al-SAB-1-10 in the present condition. However the ICP-AES result shows that the molar ratio of the Si/Al was 6, indicating dealumination and loss of acid sites. This may be the main reason for the lower benzyl alcohol conversion at the fourth recycle.

It has been discussed that the Al-SBA-1 materials have a good hydrothermal stability even after being treated in boiling water for 10 days. In order to check whether the treatment had a great effect on the catalytic activity of the Al-SBA-1 samples, here Al-SBA-1-10-HT was also tested in the Friedel–Crafts alkylation of toluene with benzyl alcohol. The results are summarized in Table 2. The conversion of benzyl alcohol reached 98% in 60 min, which is close to the Al-SBA-1-10, while the selectivity of the Al-SBA-1-10-HT was only 49% in 60 min (lower than that of the

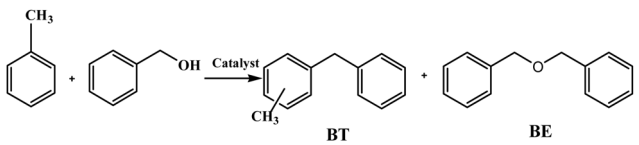

Scheme 1 Benzylation of toluene with benzyl alcohol.

Al-SBA-1-10). The selectivity finally reached 89% after 180 min, and the selectivity was slightly reduced.

4. Conclusions

Hydrothermally stable singe-crystal mesoporous Al-SBA-1 with hierarchical pore structure was successfully fabricated under alkaline condition at a high aging temperature (120 °C). By adjusting the Si/Al molar ratio in the synthesis, a series of Al-SBA-1 particles with well-ordered cubic $Pm\bar{3}n$ mesostructures were obtained. This kind of material exhibited large surface area and pore volume and highly hydrothermal stability. Friedel–Crafts alkylation of toluene with benzyl alcohol demonstrated that the Al-SBA-1 materials showed excellent catalytic properties due to the incorporated acid sites and the hierarchically mesoporous structure.

Acknowledgements

This work was supported by the National Science Foundation of China (Grant Nos. 20873070, 20973095), National Basic Research Program of China. (No. 2009CB623502), and NCET of Ministry of Education (No. NCET-07-0448) and MOE (No. IRT-0927).

Notes and references

1 S. Che, S. Kamiya, O. Terasaki and T. Tatsumi, *J. Am. Chem. Soc.*, 2001, **123**, 12089–12090.
2 J. Li, Y. Wei, Y. Deng, D. Gu, X. Yang, L. Zhang, B. Tu and D. Zhao, *J. Mater. Chem.*, 2010, **20**, 6460–6463.
3 S. Che, Y. Sakamoto, O. Terasaki and T. Tatsumi, *Chem. Mater.*, 2001, **13**, 2237–2239.
4 H. Yoshitake, T. Yokoi and T. Tatsumi, *Chem. Mater.*, 2002, **14**, 4603–4610.
5 M. J. Kim and R. Ryoo, *Chem. Mater.*, 1999, **11**, 487–491.
6 C. Yu, Y. Yu and D. Zhao, *Chem. Commun.*, 2000, 575–576.
7 A. E. Garcia-Bennett, K. Miyasaka, O. Terasaki and S. Che, *Chem. Mater.*, 2004, **16**, 3597–3605.
8 R. Ryoo and G. D. Stucky, *Nature*, 2000, **408**, 449–453.
9 T. W. Kim, R. Ryoo, M. Kruk, K. P. Gierszal, M. Jaroniec, S. Kamiya and O. Terasaki, *J. Phys. Chem. B*, 2004, **108**, 11480–11489.
10 Q. Huo, D. I. Margolese, U. Ciesla, D. G. Demuth, P. Feng, T. E. Gier, P. Sieger, A. Firouzi, B. F. Chmelka, F. Schüth and G. D. Stucky, *Chem. Mater.*, 1994, **6**, 1176–1191.
11 Q. Huo and G. D. Stucky, *Science*, 1995, **268**, 1324.
12 A. Vinu, V. Murugesan and M. Hartmann, *Chem. Mater.*, 2003, **15**, 1385–1393.
13 X. Du and J. He, *Nanoscale*, 2011, **3**, 3984–4002.
14 M. Xu, D. Feng, R. Dai, H. Wu, D. Zhao and G. Zheng, *Nanoscale*, 2011, **3**, 3329–3333.
15 Z. L. Hua, J. Zhou and J. L. Shi, *Chem. Commun.*, 2011, **47**, 10536–10547.
16 X. Guo, Y. Deng, B. Tu and D. Zhao, *Langmuir*, 2010, **26**, 702–708.
17 Z. Zhou, R. N. K. Taylor, S. Kullmann, H. Bao and M. Hartmann, *Adv. Mater.*, 2011, **23**, 2627–2632.
18 T. Sen, G. J. T. Tiddy, J. L. Casci and M. W. Anderson, *Angew. Chem., Int. Ed.*, 2003, **42**, 4649–4653.
19 D. Das, C. M. Tsai and S. Cheng, *Chem. Commun.*, 1999, 473–477.
20 J. M. Kim, S. Jun and R. Ryoo, *J. Phys. Chem. B*, 1999, **103**, 6200–6205.
21 C. Li, Y. Wang, Y. Guo, X. Liu, Y. Guo, Z. Zhang, Y. Wang and G. Lu, *Chem. Mater.*, 2007, **19**, 173–178.
22 D. Zhao, J. Feng, Q. Huo, N. Melosh, G. H. Fredrickson, B. F. Chmelka and G. D. Stucky, *Science*, 1998, **279**, 548–552.
23 S. Wu, Y. Han, Y. C. Zou, J. W. Song, L. Zhao, Y. Di, S. Z. Liu and F. S. Xiao, *Chem. Mater.*, 2004, **16**, 486–492.
24 Y. S. Ooi, R. Zakaria, A. R. Mohamed and S. Bhatia, *Catal. Commun.*, 2004, **5**, 441–445.
25 A. Vinu, D. P. Sawant, K. Ariga, M. Hartmann and S. B. Halligudi, *Microporous Mesoporous Mater.*, 2005, **80**, 195–203.
26 J. J. Chiu, D. J. Pine, S. T. Bishop and B. F. Chmelka, *J. Catal.*, 2004, **221**, 400–412.
27 P. Srinivasu, S. Alam, V. V. Balasubramanian, S. Velmathi, D. Sawant, W. Bohlmann, S. P. Mirajkar, K. Ariga, S. B. Halligudi and A. Vinu, *Adv. Funct. Mater.*, 2008, **18**, 640–651.
28 R. Ryoo and S. Jun, *J. Phys. Chem. B*, 1997, **101**, 317–320.
29 Z. Zhang, Y. Han, F. S. Xiao, S. Qiu, L. Zhu, R. Wang, Y. Yu, Z. Zhang, B. Zou, Y. Wang, H. Sun, D. Zhao and Y. Wei, *J. Am. Chem. Soc.*, 2001, **123**, 5014–5021.
30 E. Masika and R. Mokaya, *Chem. Mater.*, 2011, **23**, 2491–2498.
31 Y. Han, N. Li, L. Zhao, D. Li, X. Xu, S. Wu, Y. Di, C. Li, Y. Zou, Y. Yu and F. S. Xiao, *J. Phys. Chem. B*, 2003, **107**, 7551–7556.
32 Q. Li, Z. Wu, D. Feng, B. Tu and D. Zhao, *J. Phys. Chem. C*, 2010, **114**, 5012–5019.
33 M. Hartmann, A. Vinu, S. P. Elangovan, V. Murugesan and W. Böhlmann, *Chem. Commun.*, 2002, 1238–1239.
34 Q. Li, Z. Wu, B. Tu, S. S. Park, C. S. Ha and D. Zhao, *Microporous Mesoporous Mater.*, 2010, **135**, 95–104.
35 K. Venkatachalam, M. Palanichamy and V. Murugesan, *Catal. Commun.*, 2010, **12**, 299–303.
36 V. V. Balasubramanian, C. Anand, R. R. Pal, T. Mori, W. Böhlmann, K. Ariga, A. K. Tyagi and A. Vinu, *Microporous Mesoporous Mater.*, 2009, **121**, 18–25.
37 M. C. Liu, C. S. Chang, J. C. C. Chan, H. S. Sheu and S. Cheng, *Microporous Mesoporous Mater.*, 2009, **121**, 41–51.
38 J. G. Wang, H. J. Zhou, P. C. Sun, D. T. Ding and T. H. Chen, *Chem. Mater.*, 2010, **22**, 3829–3831.
39 X. Gu, T. Jiang, H. Tao, S. Zhou, X. Liu, J. Ren, Y. Wang, G. Lu and W. Schmidt, *J. Mater. Chem.*, 2011, **21**, 880–886.
40 C. Perego, S. Amarilli, A. Carati, C. Flego, G. Pazzuconi, C. Rizzo and G. Bellussi, *Microporous Mesoporous Mater.*, 1999, **27**, 345–354.
41 P. Botella, A. Corma, J. M. López-Nieto, S. Valencia and R. Jacquot, *J. Catal.*, 2000, **195**, 161–168.
42 S. C. Shen and S. Kawi, *J. Phys. Chem. B*, 1999, **103**, 8870–8876.
43 A. S. O'Neil, R. Mokaya and M. Poliakoff, *J. Am. Chem. Soc.*, 2002, **124**, 10636–10637.

